IntechOpen *Journals*

Digital Medicine and Healthcare Technology

REVIEW PAPER

Infrared Spectral Digital Imaging and Bone Cancer Diagnostic

Jane Anastassopoulou[1], Andreas F. Mavrogenis[2] and Theophile Theophanides[1,*]

1 International Institute of Anticancer Research, 1st km Kapandritiou-Kalamou Road, Kapandriti, Attiki, Greece

2 First Department of Orthopaedics, National and Kapodistrian University of Athens, School of Medicine, Athens, Greece

*Corresponding author. International Institute of Anticancer Research, 1st km Kapandritiou-Kalamou Road, P.O. Box 22, Kapandriti, Attiki, 19014, Greece. E-mail: theo.theophanides@gmail.com

Abstract

Scientists today are pursuing the development of non-destructive and non-invasive methods for rapid and reliable diagnosis of diseases in digital form and reduction in the need for biopsies. In this paper we review the most recent studies supporting the application of Fourier Transform Infrared (FT-IR) spectroscopy and infrared thermography or medical thermography. Both are non-destructive digital techniques, which are promising to record and discriminate the local biochemical changes that are induced by the diseases, while the examined samples do not need any special preparation. The reflected infrared radiation from the affected areas of the body strongly depends on the metabolic steps of the cancer/or any other disease, which is also related to the structural changes at a molecular level of the biological molecules during enzymatic or non-enzymatic steps of the disease. The detection of the FT-IR spectral digital "marker bands" of the obtained changes of cell, liquids or tissue components are derived from the disease in the check point. Furthermore, ImageJ analysis of the thermal imaging in cancerous area showed aggregate formation upon cancer development as it was also indicated from the FT-IR spectra.

Keywords: infrared spectroscopy, thermography, protein structure, digital diagnostic bands, precision medicine

Citation
Jane Anastassopoulou, Andreas F. Mavrogenis and Theophile Theophanides (2022), Infrared Spectral Digital Imaging and Bone Cancer Diagnostic. *Digital Medicine and Healthcare Technology* 2022(0), 1–18.

DOI
https://doi.org/10.5772/dmht.05

Copyright
© The Author(s) 2022.

This is an Open Access article distributed under the terms of the Creative Commons Attribution License (https://creativecommons.org/licenses/by/4.0/), which permits unrestricted reuse, distribution, and reproduction in any medium, provided the original work is properly cited.

Published
28 March 2022

1. Introduction

Early diagnosis of diseases is important for better treatment patients and extend their life. In this regard, diagnostics is the first step of precision medicine. Point technology in medical imaging, prevention and therapy is achieved today through technical artificial intelligence, digital processing, and handling data, as well as with totally self-made procedures [1, 2]. Moreover, innovation constitutes the application of logarithms in the handling of samples in order to derive parameters to identify correctly the results better than other methods and to combine the concepts of

Hippocratic messages with technologic "imperative" (power) [3]. In addition, the use of single and unique "bar code" or "diagnostic band" for detection of biological samples together with automation minimizes to zero the probability of false diagnostic results [4]. The development of computer technology gave the possibility to use the mathematical process of Fourier equations in order to digitalize the data to the actual spectrum. Based on the fact that the deviation to lower or higher of human's body temperature from the normal one is associated with the appearance of disease, infrared thermometers and cameras digital infrared thermal imaging cameras were developed to measure the body temperature or to scan a current area [5, 6]. In the last couple of years, many airports have used thermometers or thermocameras to detect the passengers possibly infected with Covid-19.

Nearly one hundred years after the discovery by Sir William Herschel of the thermal radiation named (*calorific rays*) or infrared radiation (infra in Latin means below, infrared = below-red) in 1800, his son John Herschel later recorded the first solar "thermogram" [7]. Hardy in 1934 described the diagnostic importance of body temperature measurement by infrared techniques and paved way for use of infrared thermography in medical science [8]. The word thermography describes the acquisition and analysis of thermal information using non-contact remote sensing [9]. The first medical images were obtained in 1959–1961 with a British prototype system, the "Pyroscan", at Middlesex Hospital in London, and the Royal National Hospital for Rheumatic Diseases [7]. In 1984, Devereaux *et al.* reported the use of liquid crystal thermography for the diagnosis of stress fractures [10]. Three years later, Hosie *et al.* published a study about the use of liquid crystal thermography for the diagnosis of scaphoid fractures supporting its use in the emergency departments as a low cost, painless and non-invasive technique with no exposure to radiation [11]. Through the years, thermal imaging cameras have been improved both on image quality and speed of image capture. Currently, modern thermal imaging is available using small reliable camera systems that can store digital images, or used online with a portable or desktop computer. Although the thermal imaging has been available for many years, however, the technique of images does not provide much information at a molecular level about the products and structural conformation.

Every object at a temperature above absolute zero emits thermal radiation [12]. Infrared imaging uses this thermal radiation with special infrared detectors to generate an image. Thermal radiation is located in the wavelength region from 0.75 to 1000 μm. The portion of the infrared spectrum that is used depends on the transmission in the atmosphere, the transmission of the used infrared optics and the spectral response of the detectors [13]. Modern infrared thermography uses real-time video/digital imaging through semiconductor focal plane arrays or micro-bolometer arrays [14, 15]. Given a blackbody (an object that absorbs all

incident radiation and radiates in a continuous spectrum) a thermal imaging camera can capture accurate remote temperature measurements. High resolution cameras with focal plane arrays of 320 × 240 pixels, a thermal sensitivity less than 50 mK and a spatial resolution of 25–50 μm ensures useful thermal and spatial details [16, 17]. Working with infrared thermography to make images of temperature changes, physicians should consider the factors that influence either the evaluation or the interpretation of the thermal images. According to Fernández-Cuevas *et al.* these factors are divided in three categories: environmental, individual (object) and technical factors [18]. Many factors can influence either the evaluation or the interpretation of the thermal images [19].

Skin surface temperature is determined by the rate of heat exchange between the surroundings and the body core [14]. Hypothalamus is the control center of core body temperature through sympathetic autonomous system. Heat is generated during metabolism and muscles during systole, and then is transported to the skin by blood flow through vessels. The sympathetic nervous system is the primary regulator of blood circulation in the skin and is therefore, the primary regulator of thermal emission [18]. The benefit of thermography is that the doctors can follow up the patients many times during the period of treatment because of absence of ionizing radiation. Thus, this method is strongly suggested for pregnant women and children [19].

In contrast to thermography, where the infrared radiation is used to increase the temperature of the irradiated body, infrared spectroscopy is based on the vibration and rotation of the atoms in molecules. The infrared radiation is interacting with the matter and the absorbed energy excites the atoms from the fundamental level to higher vibrational or rotational levels [20–24]. The infrared radiation frequencies, which are used to characterize the molecular structure are found in the region between 2.5 to 25 μm (4000–400 cm^{-1}). The development of computers and the Mickelson (Nobel 1907) interferometer led to the development of Fourier transform infrared (FT-IR) spectrometers. The use of computers and the Mickelson interferometer led to the development of Fourier transform infrared (FT-IR) spectrometers. Later, in the 1970's Theophanides [25, 26] by using Fourier transform infrared spectroscopy studied the interaction of nucleotide bases and DNA with metal ions. Living tissues are complex systems and may contain molecules named biomolecules, such as lipids, proteins, sugars, DNA, membranes while they may contain functional groups like, NH, NH_2, CH, CH_2 CH_3, COO^-, OH, PO_2^-, etc., which absorb in the same infrared region and every change of the spectrum will depend on structural changes [26–29]. The advantage of FT-IR is that a single spectrum contains the spectra of all components, which are recorded at once very rapidly.

In this article the authors will summarize the main benefits of the above-mentioned technologies, by showing examples of their potential applications.

2. *Infrared spectral digital imaging technologies*

Infrared spectral digital imaging is obtained through different steps, summarized in the following:

2.1. Thermal camera

Temperature detection is done by using IR Therma CAM camera. To minimize the false diagnostic thermographic results and to compare the temperature variations received from thermal camera with the results of other disciplinary testing methods, patients are usually allowed to stay in a stable temperature and relative humidity-controlled room, by using air condition.

2.2. FT-IR spectroscopy

FT-IR spectroscopy does not require any special sample preparation, however, the technical analyst must be careful when selecting the tissue samples. It is significant to notice that in order to obtain high quality spectra the scientists must avoid receiving formalin fixed paraffin embedded tissues [30–37]. The paraffin's absorption bands overlap the bands arising from membrane lipids and phospholipids. The spectra of the same tissue evaluated immediately after the extraction and fixation in formalin (a) or taken after paraffin incubation (b) are significantly different (figure 1). Comparison between the two spectra usually shows clearly that there are intensity changes and maximum of band shifts, while some bands have almost disappeared. Furthermore, the solute affects even the secondary structure of some remained proteins, because of solute-protein interactions (figure 1).

In FT-IR spectroscopy, when the size of the biological sample is small, the use of Attenuated Total Reflectance (ATR) apparatus gives the maximum sensitivity [36, 38]. In this case the infrared light reflects (total reflectance) many times along the sample providing an alternative of the concentration of the components (figure 2). Also, to increase the sensitivity of the FT-IR spectra the researchers can increase the number of spectra (number of scans).

Furthermore, in order to correlate the colors with the morphology and architecture of tissue sections received after surgery excision, scanning electron microscopy (SEM) has been used.

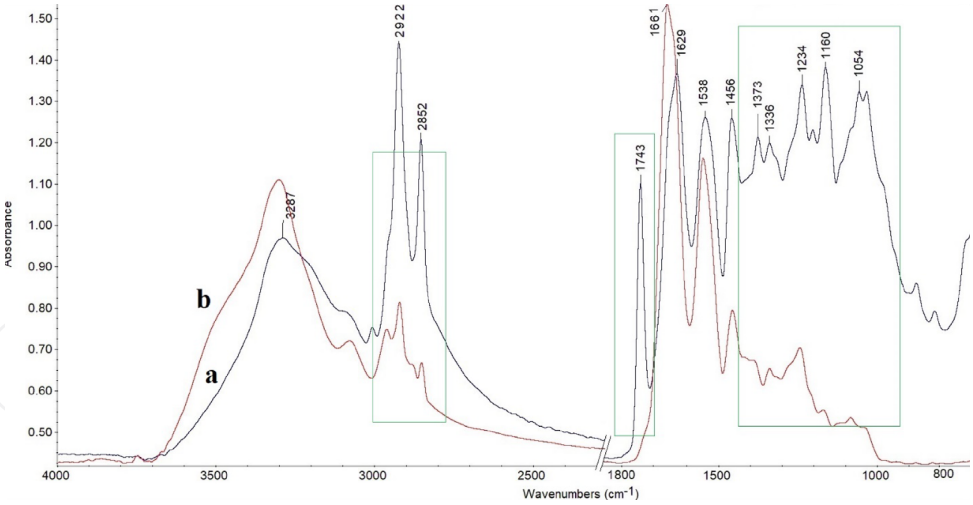

Figure 1. FT-IR spectra of cancerous bone tissues. (a) Fixation in formalin immediately after extraction and (b) the tissues were incubated in paraffin. (Nicolet 6700, 120 scans/spectra, resolution 4 cm^{-1}.) (Dr. Theophanides personal archive.)

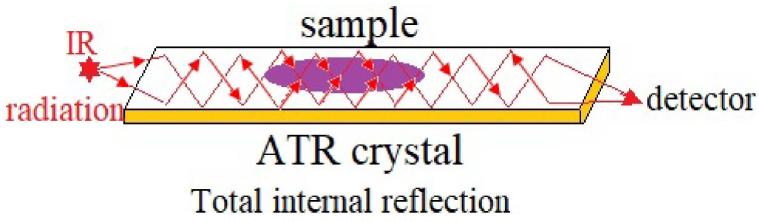

Figure 2. Schematic representation of ATR apparatus. The sample is placed in good conduct with the surface of the crystal. The IR rays pass through the sample many times, minimizing the ratio of signal to noise.

3. Applications of infrared-based technologies to bone cancer

3.1. Infrared thermal camera

Despite the high potential, it should be noted that details of the diseased tissue are not always straightly obvious. To study extensively the thermal differences and transfer these thermal data to more sensitive distinguished digital colors, ImageJ analysis software can be used. In the example provided in figure 3 [illustrating the images of the arm of a patient, who was diagnosed with metastatic cancer using X-Rays (A) and the screen with thermal camera (B)], analysis of the square region of the thermal imaging B, shows special color changes, compared to the rest of the image. Significantly, this analysis shows two areas that are illustrated like craters.

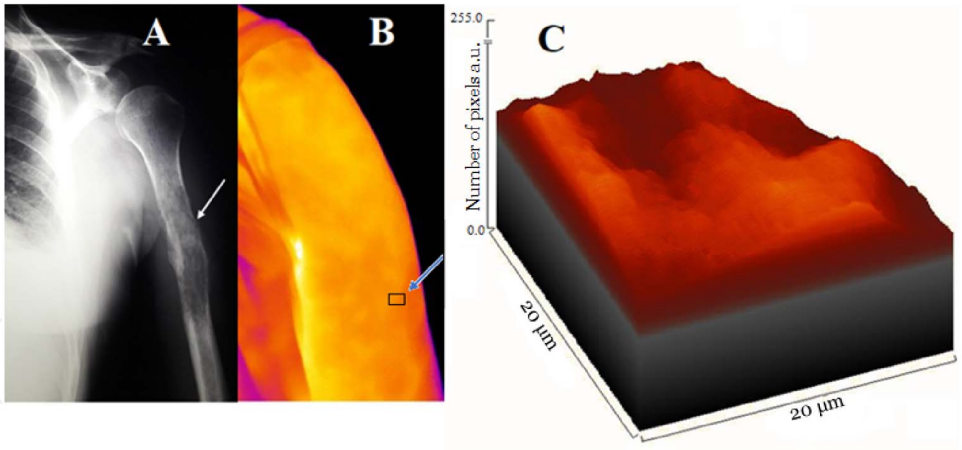

Figure 3. Images of a patient's arm who was diagnosed with metastatic cancer at the humerus using: (A) X-rays, (B) thermographic, and (C) ImageJ analysis at the square cancerous area, as it was detected using thermal camera. The two craters in (C) correspond to increased aggregates, due to cancer development. ((A,B) Dr. Mavrogenis and (C) Dr. Anastassopoulou's personal archive.)

It has been observed that the crater-like form appears in cancerous tissue, but also as atherosclerotic plaques of patients [24]. It was found that the tissues are rich in lipophilic environment and amyloid proteins.

3.2. SEM morphology

A further step of investigation, to better understand how the disease affects the tissue, the morphology and architecture of the cancerous bone can be analyzed, as mentioned, using SEM. SEM obtains high resolution analysis of the biopsies close to native state, without need of coating. In figure 4, the architecture of cancerous bone is illustrated; remarkably and similarly to what was expected in molecular pathology, the analysis was carried out on sections immediately corresponding to the ones examined for histopathological diagnosis. SEM can investigate and demonstrate the heterogeneity of a given tissue.

The combination with EDX (energy diffraction X-Rays) permits us to discriminate and characterize the element composition in very low small area, as is a biopsy section. In case of bones, for example, by determining the relative concentrations of the calcium (Ca) and phosphorous (P) atoms in the detected area of biopsy and calculate the ratios [Ca]:[P] it is easy to diagnose the osteoporotic or calcified regions due to a disease. X-Ray diffraction (XRD) can demonstrate that the hydroxyapatite loses its stoichiometric chemical composition, $[(Ca_{10}(PO_4)_6(OH)_2)]$ and crystals of inorganic calcium phosphate salt $(Ca_3(PO_4)_2$

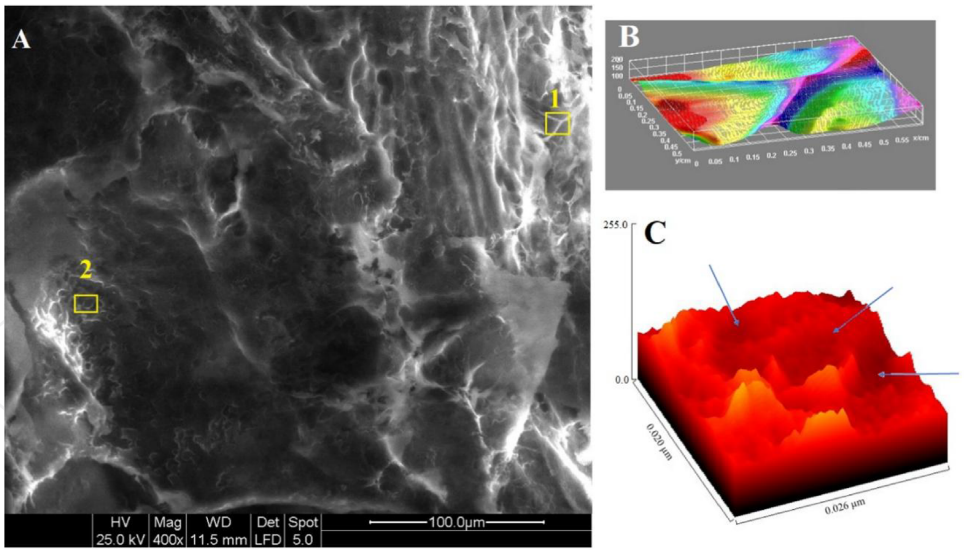

Figure 4. Scanning electron microscopy (SEM) an illustration of the morphology and architecture of cancerous bone section. The bright places correspond to hydroxyapatite in the bone, which are reduced. (B) and (C) are the results of ImageJ analysis of cross-linked proteins and demineralized areas, respectively. The square surrounded areas 1 and 2 show the cross-linked proteins, respectively. Scale 100 µm, Mag 200×. (Dr. Anastassopoulou's personal archive.)

are produced, enhancing further the bone resorption. Cross-linked proteins, damaged proteins, fibers and many other abnormalities are also detected.

ImageJ analysis of the outer-line square areas, where the cross-links of proteins are in SEM pictures, shows in our example that the proteins do not bind to hydroxyapatite. The formation of characteristic cross-links indicates that oxidative stress is present as cancer associated feature, and that free radicals are involved in the phenomenon [39, 40]. Upon oxidative stress the free radicals, which are mainly hydroxyl radicals (HO.) which by interacting with proteins produce proteins free radicals and finally form dimers, cross-links, fibrils, etc. [39, 40].

3.3. FT-IR spectra of cancerous bone tissues

In the infrared spectral region between 4000–3000 cm^{-1} are located the characteristic stretching vibrational modes of the υOH frequencies obtained from hydroxyapatite and other overlapping hydrogen bonded bands of this group and the υNH frequency of proteins and DNA (figure 5). In bone cancer, the band intensities of vibration of υOH and υNH modes are obtained from the spectra originated from the cancerous bones suggesting the damage of both hydroxyapatite and collagen molecules of bone tissues [41–44]. From the shift of the maximum, of the υNH

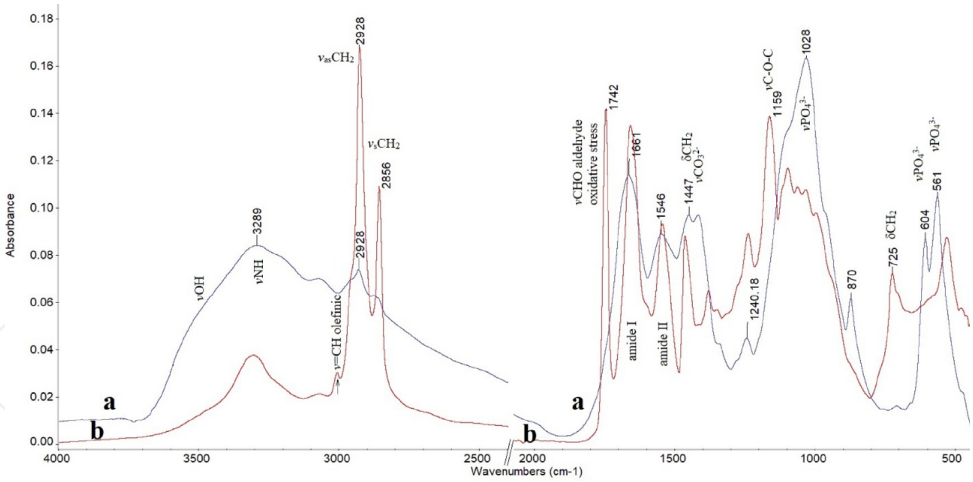

Figure 5. FT-IR spectra of slices from healthy bone (a) and cancerous bone (b) in the spectral region 4000–500 cm^{-1}. (Dr. Theophanides' personal archive.)

absorption band to higher wavenumbers we obtain the increasing number of free NH groups [31, 42–45].

3.4. Data integration for advanced diagnostics

In the presented example of bone cancer, in the fingerprint region 3000–2850 cm^{-1} the observed bands are assigned to antisymmetric $v_{as}CH_3$, (~2957 cm^{-1}) and symmetric stretching v_sCH_3 (~2871 cm^{-1}) vibrations of terminal methyl groups. These bands are shoulders in the spectra of normal bones. On the contrary, the stretching v_sCH_3 bands are weak and have almost disappeared. Bands arising from the stretching vibration of antisymmetric $v_{as}CH_2$ and symmetric v_sCH_2 modes of methylene groups located at 2928 cm^{-1} and 2858 cm^{-1}, respectively, are pronounced in the spectra of cancerous bones (figure 5b). The νCH_2 stretching absorption bands are very sensitive and the peak position depends not only on the size of the alkyl chain but also on the surrounding environment [41–43] and give fundamental information for the changes in membrane fluidity upon disease development and formation. In the present case it was indicated that cancer development has influenced the lipophilic environment and that the hydrophobic interactions between the hydrocarbon chains, as well as between intermembrane proteins changed their order-disorder puckering provoking the lipid aggregate formation [41]. This change was observed in many cancers and the ratio of the band intensities $[v_{as}CH_3]/[v_{as}CH_2]$ depends on the progression of the cancer development [42, 43].

In the spectral region 1800–1500 cm^{-1} the intensities of all bands are very sensitive and are strongly affected by the disease [42–49]. The high intensity absorption "marker band" at 1742 cm^{-1} is originated from νRHCO aldehydic group,

confirming the suggestion that oxidative modification of proteins by ROS (reactive oxygen species) took place upon cancer development [47–50]. The intensity of this particular band is also related to the presence of inflammation. The protein carbonyl group has been used as indicator "marker band" for protein oxidation and it was observed in several other diseases, such as aortic valve calcification, diabetes, cancer, arthritis, colitis, inflammatory of bowel [29, 36, 46, 51–54]. This band is well differentiated from the stretching vibration of the protein carbonyl group υC=O, which absorbs at lower frequencies.

The peptide bonds –CO-NH– of proteins give several absorption amide bands of which the most intense and sensitive are the amide I at 1655 cm^{-1} and amide II near 1541 cm^{-1} (see figure 5) the region 1700–1500 cm^{-1} as shown in figure 6. Amide I is resulted from the in-plane carbonyl stretching (υC=O) vibration and bending δNH vibration. The amide II band is attributed to bending vibration of the δNH modes coupled to υC–N stretching. The protein is named from the Greek words *protos* = first, and *ina* = fiber, the first-fiber) are very complicated molecules and the building blocks are the amino acid residues which are linked by peptide bonds through hydrogen bonds to form the backbone strands of the helices. The hydrogen bond is a molecular interaction of donor–acceptor type and is distinctly directional, specific and stronger than Van der Waals forces and much weaker than the usual chemical bonds. The strength of the hydrogen bond is affected from various conditions, such as temperature, pH and fluidity of the close local environment [55, 56]. This property makes the amide I band to be useful for diagnosis. The intensity of the amide I band is stronger than amide II.

Comparison between the spectral amide I and amide II regions also shows considerable differences in shape and absorption intensities between normal vs. neoplastic tissue. These bands are strongly affected from the progression of cancer and can be used as distinct digital "marker bands" for the progression of cancer, the band intensities decrease, while the bands become broad. This means that upon cancer development the proteins change their secondary molecular structure. The shape and bandwidth of the amide I and amide II bands of the cancerous bone (figure 5b) indicates that an infrared spectrum has overlapping bands and leads to the suggestion to further analyze the spectra.

The application of deconvolution spectra or first derivatives' or resolved analysis using the software of the instrument can differentiate the absorption bands and contribute to detailed studies and information on the proteins.

The deconvolution analysis allows us to appreciate that upon disease progression the proteins change their secondary structure from α-helix, while the overlapping bands are attributed to antiparallel (↑↓) and parallel (⇈) β-sheets. These conformations correspond to amyloid proteins. The obtained β-sheets are enhanced

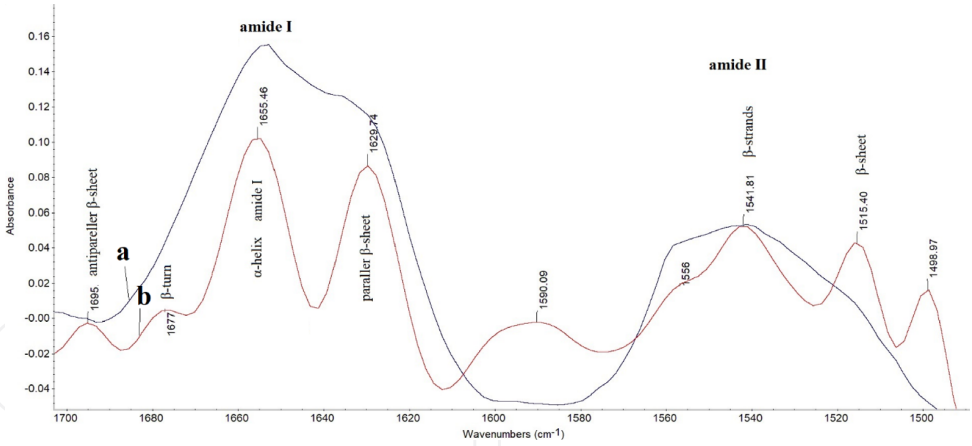

Figure 6. (a) FT-IR spectra in the spectral region 1700–1500 cm^{-1}; (b) deconvolution of the spectra reveals distinct bands, which correspond to antiparallel and parallel β-sheets. (Dr. Theophanides' personal archive.)

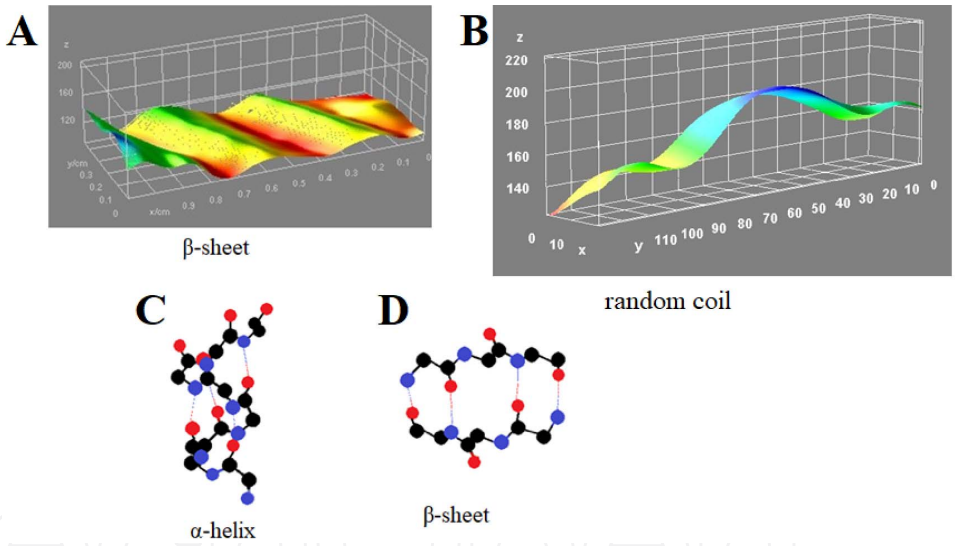

Figure 7. ImageJ results of proteins obtained in SEM presented in figure 3: (A) β-sheet conformational protein structure, (B) random coil. (C) and (D) schematic presentation of the hydrogen bonds (C) α-helix, (D) β-sheet conformations (Dr. Anastassopoulou's personal archive).

from the enriched lipophilic environment, as was suggested from the increasing of the intensity bands of the antisymmetric and symmetric stretching vibrations of methylene groups $\upsilon_{as,s}CH_2$. It seems that the lipophilic environment changes the dipole moment of the peptide bond and change the orientation of amino groups (NH) to carbonyl (C=O) forming self assembly as it is shown in (figures 3 and 7).

The extended β-strands can interact also between each other by hydrogen bonds changing the conformation of the proteins, while, the lipophilic environment reverses the chain direction producing aggregates. Accumulation of aggregated amyloid proteins inhibits the regeneration of the bone leading to osteoporosis and osteolysis. It is known that the conformation of proteins is associated with the quality of biological hydroxyapatite of the bones [53, 57–60].

Schmidt *et al.* [61] have shown that the quality of the human bones depends on the cross-links and fibril formation. The formation of protein aggregates promotes the increase of the local temperature compared with the bone and thus by developing suitable software for detection of the damage with thermal camera, one can determine this difference as shown in figure 2A. SEM illustrations further show protein cross-links and fibril leading to inhibition of biological formation hydroxyapatite. Finally, the FT-IR spectra can show the formation of inorganic hydroxyapatite [57, 61–64] supporting the reduction of the mechanical properties of the bones increasing the risk of bone fractures. The changes obtained by subtraction of the FT-IR spectra of healthy and cancerous bones can aid in more detailed studies on the effect of the disease in the bones. ImageJ 3D analysis of damaged proteins received from SEM, can serve, as in our example to confirm, and validate the results from the above FT-IR spectra. Based on previous observations, FT-IR spectroscopy seems suitable to reveal the insights of the protein secondary structure composition.

The band at 1028 cm^{-1} corresponds to stretching vibration of phosphate υPO_4^{3-} groups of biological hydroxyapatite [59, 60] and is almost disappeared upon cancer development. Studying the bone sections with micro-FT-IR spectrometer combining with microscope it is possible to have the topography/micro-architecture of the high non-homogeneous tissues. Calculation of the ratio of the phosphate υPO_4^{3-} (1028 cm^{-1}) to amide I (1655 cm^{-1}) peaks permitted to determine the mineral matrix at each site of the micro-FT-IR spectroscopic analysis.

The variation of the minerals and proteins in the bone can also be evaluated (figure 8).

The decrease of the concentration in hydroxyapatite is a sign of the loss of hydroxyapatite during the cancer development [65–69], which changes the bone properties and is remodeling, and usually presents in agreement with clinical data.

The region 1300–900 cm^{-1} is a very important spectral region and gives details on the phosphate mode about the progression of the cancer. The most important bands in this region are the stretching vibrations resulting from υPO_2^- of phospholipids and of DNA [25–28, 66, 67], the sugar-phosphate bands of DNA ribose [66–69] and the stretching vibration of the glycosylic bonds –O–C–O–.

The band at about 1240 cm^{-1} increases in the spectra of cancerous bone indicating that there is an increase in stretching of the phosphate ribose groups.

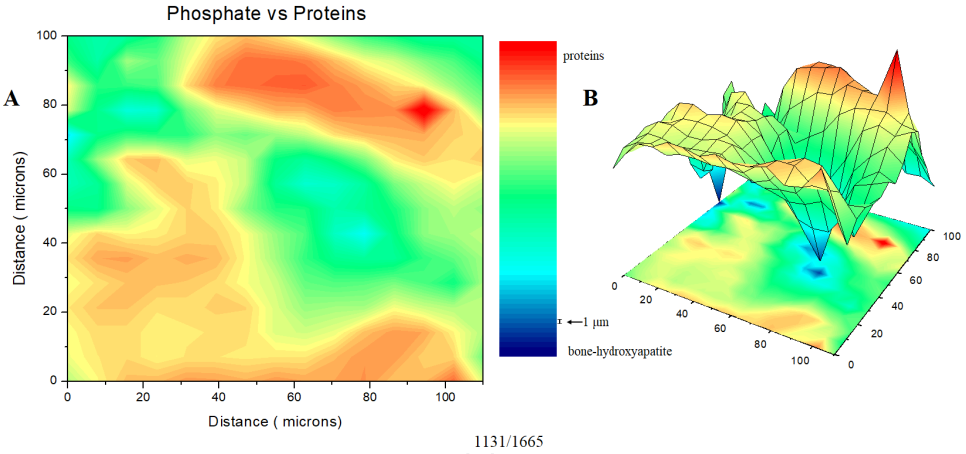

Figure 8. Synchrotron FT-IR imaging of cancerous bone. (A) and (B) correspond to 2D and 3D distribution of hydroxyapatite (blue) and protein (red) composition. The deep colors correspond to high concentrations; the color scale is the in between concentrations. The spectra were collected in transmission mode with a square aperture of 8 × 8 μm. (Dr. Theophanides' personal archive.)

The pentose phosphate is a pathway in the metabolism of cancer [68–70]. The implication of NADH in pentose phosphate generation elevates the ATP generation of cancer cells [68, 69] and leads to the suggestion that oxidative stress is involved in cancer development. This high metabolic pathway increases the temperature of the body, which could be detected with an infrared camera. The intense band at 1159 cm^{-1} is assigned to stretching vibration of *v*–O–C–O– glycosylic mode and is predominant in the spectra of cancers. This band can be used as a digital "marker band" for cancer detection [41, 44, 71, 72]. The band is also related to protein glycosylation and advanced glycation products (AGEs) [36, 71, 72]. Finally, the band at about 1079 cm^{-1} is assigned to exocyclic –C–O–C (oxygen bridges) [35, 44, 45].

4. Conclusions

In this paper the non destructive methods, infrared thermography and Fourier transform infrared (FT-IR) spectroscopy are described with specific emphasis on their role in bone cancer diagnostics. They can detect the changes which affect the body's temperature with those of the molecular structure of cells and tissues of the body. The reflected infrared radiation from the affected areas of the body strongly depends on the metabolic steps of the cancer/or any other disease, which is also related to the structural changes at a molecular level of biological molecules during enzymatic or non enzymatic steps of the disease. The detection of the FT-IR spectral digital "marker bands" of the obtained changes of cell, liquids or tissue components derived from the disease in the check point could help to correlate with the

corresponding temperature transferred to surface from the influenced site growth. The development of models, sensitive software, protocols and algorithms for early diagnosis of diseases, such as cancer, sarcomas, impending pathological fractures and histological diagnosis (biopsy) is of paramount importance specifically to the high heterogeneity and complex microenvironment of the human tissues [73–88]. In this respect, infrared thermal and infrared spectroscopic digital imaging data can be used to develop softwares that will be the fingerprint of specific diseases. Fingerprints are supported by computers and could be transferred to pixels for high resolution color classifications that will act as barcodes for early *in vivo* diagnosis of diseases.

Conflicts of interest

There is no conflict of interest.

References

1 **Giamougiannis P.**, **Morais C. L. M.**, **Rodriguez B.**, **Wood N. J.**, **Martin-Hirch P. L.**, **Martin F. L.** Detection of ovarian cancer (±neo-agjuvant chemotherapy effects) via ATR-FTIR spectroscopy: comparative analysis of blood and urine biofluids in a large patient cohort. ***Anal. Bioanal. Chem.***, 2021; **413**(20): 5095–5107. doi:10.1007/s00216-021003472-8. PMID: 34195877. PMCID: PMC8405472.

2 **Errani C.**, **Tsukamoto S.**, **Mavrogenis A. F.** Imaging analyses of bone tumors. ***JBJS Rev.***, 2020; **8**(3): e0077. doi:10.2106/jbjs.rvw.1900077. PMID: 32149935.

3 **Marketos S. G.**, **Skiadas P. K.** The modern hippocratic tradition. Some messages for contemporary medicine. ***Spine (Phila Pa 1976)***, 1999; **24**(11): 1159–1163. doi:10.1097/00007632-199906010-00019. PMID: 10361669.

4 **Aggarwal R.**, **Soounderajah V.**, **Martin G.**, **Ting D. S. W.**, **Karthikesalihgam A.**, **King D.**, **Ashrafian H.**, **Darzi A.** Diagnostic accuracy of deep learning in medical imaging: a systematic review and meta-analysis. ***NPJ Digit. Med.***, 2021; **4**: 65. https://doi.org/10.1038/s41746-021-00438-z.

5 **Wang R.**, **Wang Y.** Fourier transform infrared spectroscopy in oral cancer diagnosis. ***Int. J. Mol. Sci.***, 2021; **22**(3): 1206. doi:10.3390/ijms22031206, PMCID: PMC7865696, PMID: 33530491.

6 **Laštovička-Medin G.** Thermal imaging as a tool for pattern recognition and anomaly studies: identifying the changes in the condition of an object over time by spotting a trend of hanging temperatures. ***RAD Conf. Proc.***, 2017; **2**: 198–206. www.rad-proceeding.org.

7 **Ring E. F. J.**, **Mcevoy H.**, **Jung A.**, **Zuber J.**, **Machin G.** New standards for devices used for the measurement of human body temperature. ***J. Med. Eng. Technol.***, 2010; **34**(4): 249–253. http://www.informaworld.com/journals. doi:10.3109/03091901003663836.

8 **Hardly J. D.** The radiation of heat from the human body III. The human skin as black-body radiation. ***Clin. Invest.***, 1934; **13**(4): 615–620. doi:10.1172/JCI100609.

9 **Habash R.** BiomElectroMagnestics: Human Safety and Biomedical Applications. Second edition, Boca Raton: CRC Press, Taylor & Francis Group, 2020; p. 438.

10 **Ring E. F. J.** The historical development theo of thermometry and thermal imaging in medicine. ***J. Med. Eng. Technol.***, 2006; **30**(4): 192–198.

11 **Devereaux M. D.**, **Parr G. R.**, **Lachmann S. M.**, **Page-Thomas P.**, **Hazleman B. L.** The diagnosis of stress fractures in athletes. ***J. Am. Med. Assoc.***, 1984; **252**(4): 531–533.

12 **Hosie K.**, **Wardrope J.**, **Crosby A.**, **Ferguson D.** Liquid crystal thermography in the diagnosis of scaphoid fractures. ***Arch. Emerg. Med.***, 1987; **4**(2): 117–120.

13 **Jones B. F.** A reappraisal of the use of infrared thermal image analysis in medicine. ***IEEE Trans. Med. Imaging***, 1998; **17**(6): 1019–1027.

14 **Mollmann K. P.**, **Vollmer M.** Infrared thermal imaging as a tool in university physics education. ***Eur. J. Phys.***, 2007; **28**: S37–S50.

15 **Maldague X.** Theory and Practice of Infrared Technology for Nondestructive Testing. New York: John Wiley and Sons, 2001.

16 **Oda N.**, **Kurhina S.**, **Miyoshi M.**, **Doi K.**, **Sudou T.**, **Morimoto T.**, **Goto H.**, **Sasaki T.** Microboometer terahertz focal array and camera with improved sensitivity in the sub-terahertz region. ***J. Infrared Milli. Terahz. Waves***, 2015; **36**: 947–960. https://doi.org/10.1007/s10762-015-0184-2.

17 **Ring E. F. J.**, **Ammer K.** The technique of infrared imaging in medicine. ***Thermol. Intern.***, 2000; **10**(1): 7–14.

18 **Fernández-Cuevas I.**, **Marins J. C. B.**, **Lastras J. A.**, **Carmona P. M. G.**, **Cano S. P.**, **Miguel García-Concepción A.**, **Sillero-Quintana M.** Classification of factors influencing the use of infrared thermography in humans: a review. ***Infrared Phys. Technol.***, 2017; **71**: 28–55. ISSN 1350-4495, https://doi.org/10.1016/j.infrared.2015.02.007.

19 **Zaproudina N.**, **Varmavuo V.**, **Airaksinen O.**, **Narhi M.** Reproducibility of infrared thermography measurements in healthy individuals. ***Physiol. Meas.***, 2008; **29**: 515–524.

20 **Theophanides T.** Infrared and Raman Spectroscopy of Biological Molecules. NATO Advanced Study Institute Series. Holland, Boston: USA, London, England: D. Reidel Publishing Company, Dordrecht, 1978. https://doi.org/10.1007/978-94-009-9412-6.

21 **Theophanides T.** Fourier Transform Infrared Spectroscopy. Industrial, Chemical and Biochemical Applications. Dordrecht, Boston, Lancaster: D. Reidel Publishing Company, 1984. doi:https://doi.org/10.1007/978-94-009-6418-1.

22 **Theophanides T.** Infrared Spectroscopy-Life and Biomedical Science. InTech Open, 2012. doi:10.5772/2055.

23 **Theophanides T.** Infrared Spectroscopy-Materials Science, Engineering and Technology. InTech Open, 2012. doi:10.5772/2055, ISBN 978-953-51-0537-4.

24 **Theophanides T.** Infrared Spectroscopy-Anharmonicity of Biomolecules, Crosslinking of Biopolymers, Food Quality and Medical Applications. InTech Open, 2015. ISBN: 9535117378.

25 **Theophanides T.** In: Theophanides T. (ed.), Vibrational Spectroscopy of Metal Nucleic Acid Systems, Infrared and Raman Spectroscopy Applied to Biological Molecules. Dodrecht, Holland: D. Reidel Publishing Co, 1978; pp. 205–223.

26 **Theophanides T.** Fourier transform infrared spectra of calf thymus DNA and its reactions with anticancer drug *cis*-platin. ***Appl. Spectrosc.***, 1981; **35**: 461–465.

27 **Anastassopoulou J.**, **Theophanides T.** Aquation of metal ions and infrared and Raman spectra of metal complexes and their interaction with DNA components—A vibrational study of metal–DNA interactions. In: Muntean C. M., Hernanz A., Bratu J. (eds), Insights into Vibrational Spectroscopy of Nucleic Acids and their Complexes. 37/661 (2), Fort P.O., Trivandrum-695 023, Kerala, India: Transworld Research Network Publishers, 2009; pp. 47–65, Chapter 3, ISBN: 978-81-7895-407-3.

28 **Theophanides T.**, **Anastassopoulou J.** The use of Fourier transform infrared (FT-IR) spectroscopy in the structural analysis of nucleic acids. In: Vergoten G., Theophanides T. (eds), Biomolecular Structure and Dynamics: Recent Experimental and Theoretical Advances. The Netherland: Kluwer Academic Publishers, 1997; pp. 273–284, ISBN: 9789401154840.

29 **Kyriakidou M.**, **Anastassopoulou J.**, **Tsakiris A.**, **Koui M.**, **Theophanides T.** FT-IR spectroscopy study in early diagnosis of skin cancer. ***In Vivo***, 2017; **31**(6): 1131–1137.

30 **Snyder R. G.** Vibrational spectroscopy of crystalline *n*-paraffins part I. Methylene rocking and wagging modes. ***J. Mol. Spectrosc.***, 1960; **4**: 411–434.

31 **Bellamy L. J.** Infrared Spectroscopy of Complex Molecules. London: Methuen, 1975. https://doi.org/10.1007/978-94-011-6520-4.

32 **Anastassopoulou J.**, **Kyriakidou M.**, **Mamareli V.**, **Tanis O.**, **Rallis M.** The influence of UV irradiation on diabetic mice skin. A vibrational FT-IR and Raman spectroscopic study. ***Chromatogr. Spectrosc. Tech.***, 2019; **2**(1): 21–27.

33 **Anastassopoulou J.**, **Mamareli V.**, **Mylonas E.**, **Kolovou P.**, **Mamarelis I.**, **Kotoulas C.**, **Mamareli C.**, **Kotoulas S.**, **Koutoulakis E.**, **Spiliopoulos K.**, **Theophanides T.** Infrared spectroscopic study and mathematical simulations of carotid atherosclerosis. ***In Vivo***, 2022; **33**(1): 89–1972. doi:10.21873/invivo.12690.

34 **Anastassopoulou J.**, **Kyriakidou M.**, **Malesiou E.**, **Rallis M.**, **Theophanides T.** Infrared and Raman spectroscopic studies of skin molecular disorders and cancer. ***In Vivo***, 2019; **33**: 567–572.

35 **Mamareli V.**, **Tanis O.**, **Anastassopoulou J.**, **Kyriakidou M.**, **Mamareli C. H.**, **Koui M.**, **Theophanides T.**, **Mamarelis I.** The role of oxidative stress on molybdenum enzymes and ischemic reperfusion injury in hyperuricaemic patients. An infrared spectroscopic study. ***Eur. J. Mol. Clin. Med.***, 2019; **6**(1): 20–25. doi:http://doi.org/10.5334/ejmcm.

36 **Megaloikonomos P.**, **Panagopoulos G. N.**, **Bami M.**, **Igoumenou V. G.**, **Dimopoulos L.**, **Milonaki A.**, **Kyriakidou M.**, **Mitsiokapa E.**, **Anastassopoulou J.**, **Mavrogenis A. F.** Harvesting, isolation and differentiation of rat adipose-derived stem cells. ***Curr. Pharm. Biotechnol.***, 2018. doi:10.2174/1389201019666180411810132 3.

37 **Brandenburg K.**, **Kusumoto S.**, **Seydel U.** Conformational studies of synthetic lipid A analogues and partial structures by infrared spectroscopy. ***Biochim. Biophys. Acta (BBA)***, 1997; **1329**: 183–201.

38 **Harrick N. J.** Internal Reflection Spectroscopy. New York: Willey & Sons, Inc., 1967. IRS-671.

39 **Halliway B.**, **Gutteringe J. M. C.** Free Radical in Biology and Medicine. Second edition, New York: Oxford University Press, 1989.

40 **Mamarelis I.**, **Koutoulakis E.**, **Kotouas C.**, **Dritsa V.**, **Mamareli V.**, **Anastassopoulou J.** The role of oxidative stress on amyloid-like formation and aortic valve calcification. ***Hell. J. Cardiol.***, 2017; 7(2): 84–96. doi:10.1016/j.hjc.2016.09.011.

41 **Arrondo J. L. R.**, **Goñi F. M.** Infrared spectroscopic studies of membrane lipids. In: Vergoten G., Theophanides T. (eds), Biomolecular Structure and Dynamics. NATO ASI SeriesKluwer Academic Publishers, 1999; pp. 229–242.

42 **Kolovou P.**, **Anastassopoulou J.** Synchrotron FT-IR spectroscopy of human bones. The effect of aging. In: Tsakanov V., Wiedemann H. (eds), Brilliant Light in Life and Material Sciences. New York Inc.: Springer-Verlag, 2007; pp. 267–272.

43 **Anastassopoulou J.**, **Kolovou P.**, **Mavrogenis A.** Bone and cancer. A synchrotron micro-infrared study. In: Collery P. H., Maymard J., Khassanova L., Theophanides Collery T. (eds), Metal Ions Biology and Medicine. vol. 10, 2008; pp. 210–213.

44 **Anastassopoulou J.**, **Boukaki E.**, **Conti C.**, **Ferraris P.**, **Giorgini E.**, **Rubini C.**, **Sabbatini S.**, **Theophanides T.**, **Tosi G.** Microimaging FT-IR spectroscopy on pathological breast tissues. ***Vibrational Spectroscopy***, 2009; **51**: 270–275.

45 **Conti C.**, **Ferraris P.**, **Giorgini E.**, **Rubini C.**, **Sabbatini S.**, **Tosi G.**, **Anastassopoulou J.**, **Arapantoni P.**, **Boukaki E.**, **Theophanides T.**, **Valavanis C.** FT-IR microimaging spectroscopy: discrimination between healthy and neoplastic human colon tissues. ***J. Mol. Struc.***, 2008; **881**: 46–51.

46 **Casbas-Hernandez P.**, **D'Arcy M.**, **Roman-Perez E.**, **Brauer H. A.**, **McNaoughton K.**, **Miller S. M.**, **Chhetri R. K.**, **Oldenburg A. L.**, **Fleming J. M.**, **Amos K. D.**, **Makowski L.**, **Troester A.** Role of HGF in

epithelial–stromal cell interactions during progression from benign breast disease to ductal carcinoma in situ. ***Breast Cancer Res.***, 2013; **15**(5): R82. doi:10.1186/bcr3476.

47 **Kotoulas C.**, **Mamarelis I.**, **Koutoulakis E.**, **Kyriakidou M.**, **Mamareli V.**, **Tanis O.**, **Malesiou E.**, **Theophanides T.**, **Anastassopoulou J.** The influence of diabetes on atherosclerosis and amyloid fibril formation of coronary arteries. A FT-IR spectroscopic study. ***Hell. J. Atheroscler***, 2017; **8**: 15–29.

48 **Mamareli V.**, **Tanis O.**, **Anastassopoulou J.**, **Kyriakidou M.**, **Mamareli C. H.**, **Koui M.**, **Theophanides T.**, **Mamarelis I.** The role of oxidative stress on molybdenum enzymes and ischemic reperfusion injury in hyperuricaemic patients. An infrared spectroscopic study. ***Eur. J. Mol. Clin. Med.***, 2019; **6**(1): 20–25. doi:http://doi.org/10.5334/ejmcm.268.

49 **Anastassopoulou J.**, **Kyriakidou M.**, **Nisiakis P.**, **Papatheodorou G.**, **Rallis M.**, **Theophanides T.** The environmental effects of lead concentrations on protein and DNA structure in epileptic patients from an infrared spectroscopic study. ***J. Basic Appl. Sci.***, 2019; **15**: 56–63.

50 **Anastassopoulou J.**, **Mamarelis I.**, **Theophanides T.** Study of the development of carotid artery atherosclerosis upon oxidative stress using infrared spectroscopy and scanning electron microscopy. ***OBM Geriatrics***, 2021; 5(4). doi:10.21926/obm.geriatr.2104180, PMCID: PMC831197.

51 **Dubois J.**, **Shaw R. A.** IR spectroscopy in clinical and diagnostic applications. ***Anal Chem.***, 2004; **76**(19): 360A–367A.

52 **Dalle-Donne I.**, **Rossi R.**, **Giustarini D.**, **Milzani A.**, **Colombo R.** Protein carbonyl groups as biomarkers of oxidative stress. ***Clin. Chim. Acta***, 2003; **329**: 23–38.

53 **Akbulut H.**, **Akbulut K. G.**, **Icli F.**, **Büyükcelic A.** Daily variations of plasma malondialdehyde levels in patients with early breast cancer. ***Cancer Detect. Prev.***, 2003; **27**(2): 122–126. PMID: 12670523, doi:10.1016/s0361-090x(03)00029-1.

54 **Mohideen K.**, **Sudhara U.**, **Balakrishnan T.**, **Almasri M. A.**, **Al-Almari M. M.**, **Al Dira H. S.**, **Suhlili M.**, **Dubey A.**, **Mujoo S.**, **Khurshid Z.**, **Raj A. T.**, **Patil S.** Malondialdehyde, an oxidative stress marker in oral squamous cell carcinoma-A systematic review and meta-analysis. ***Curr. Issues Mol. Biol.***, 2021; **43**: 1019–1035. https://doi.org/10.3390/cimb43020072. doi:10.3390/cimb43020072.

55 **Barth A.**, **Zscherp C.** What vibrations tell us about proteins. ***Q. Rev. Biophys.***, 2002; **35**(4): 369–430. doi:10.1017/s0033583502003815.

56 **Barth A.** Infrared spectroscopy of proteins. ***Biochim Biophys. Acta***, 2007; **1767**(9): 1073–1101. doi:10.16/jbbabio.2007.06.004.

57 **Anastassopoulou J.**, **Kyriakidou M.**, **Kyriazis S.**, **Mavrogenis A.**, **Mamareli V.**, **Mamarelis I.**, **Petra M.**, **Malesiou E.**, **Kotoulas C.**, **Kolovou P.**, **Koutoulakis E.**, **Markouizou A.**, **Theophanides T.** Oxidative stress in aging and disease development studied by FT-IR spectroscopy. ***J. Machanisms Age Dev.***, 2018; **172**: 107–114. doi:10.1016/j.mad.2017.11.009.

58 **Fringeli U. P.**, **Günthar. H. H.** Infrared membrane spectroscopy. In: Grell E. (ed.), Membrane Spectroscopy. Berlin, Heidelberg, New York: Spinger-Verlag, 1981.

59 **Petra M.**, **Anastassopoulou J.**, **Theologis T.**, **Theophanides T.** Synchrotron micro-FT-IR spectroscopic evaluation of normal paediatric human bone. ***J. Mol. Struct.***, 2005; **78**: 101–110.

60 **Petra M.**, **Anastassopoulou J.**, **Yfantis D.**, **Theophanides T.** FT-IR spectra of human bones. In: Greve J., Puppels G. J., Otto C. (eds), Spectroscopy of Biological Molecules: New Directions. Dordrecht: Kluwer Academic Publishers, 1999; p. 55.

61 **Schmidt F. N.**, **Zimmermann E. A.**, **Campbell G. M.**, **Sroga G. E.**, **Püschel K.**, **Amling M.**, **Tang S. Y.**, **Vashishth D.**, **Busse B.** Assessment of collagen quality associated with non-enzymatic cross-links in human bone using Fourier-transform infrared imaging. ***Bone***, 2017; **97**: 243–251. doi:10.1016/j.bone.2017.01.015. Epub 2017 Jan 18.

62 **Miller L. M.**, **Carlson C. S.**, **Carr G. L.**, **Chance M. R.** A method for examining the chemical basis for bone diseases: synchrotron infrared microscopy. ***Cell Mol. Biol.***, 1988; **44**: 117–127.

63 **Boskey A.**, **Medelson R.** Infrared analysis of bone in health and disease. ***J. Biomed. Opt.***, 2005; **19**(3): 031102. https://doi.org/10.1117/1.1922927.

64 **Paschalis E. P.**, **Medelson R.**, **Boskey A.** Infrared assessment of bone quality: a review. ***Clin. Orthop. Relat. Res.***, 2011; **469**(8): 2170–2178. doi:10.1007/s11999-010-1751-4, PMCID: PM3126953, PMID: 21210314.

65 **Boskey A. L.**, **Spevak L.**, **Weinstein R. S.** Spectroscopic markers of bone quality in alendronate-treated postmenopausal women. ***Osteoporos Int.***, 2009; **20**(5): 793–800. doi:10.1007/s00198-008-0725-9.

66 **Theophanides T.** Interactions des Acides Nucleiques avec les. ***Metaux Can. J. Spectr.***, 1981; **26**: 165–179.

67 **Tajmir-Riahi H. A.**, **Theophanides T.** An FT-IR study of DNA and RNA conformational transitions at low temperatures. ***J. Biomol. Struct. Dyn.***, 1985; **3**: 537–542.

68 **Legal J.-M.**, **Manfait M.**, **Theophanides T.** Applications of FT-IR spectroscopy in structural studies of cells and bacteria. ***Mol. Structure***, 1991; **242**: 397–407.

69 **Patra K. C.**, **Hay N.** The pentose phosphate pathway and cancer. ***Trends Biochem. Sci.***, 2014; **39**(8): 347–354. doi:10.1016/j.tibs.2014.06,005. PMCID: PMC4329227, NIHMSID: NIHMS614191, PMID: 25037503.

70 **Zhelev Z.**, **Aoki I.**, **Lazarova D.**, **Vlaykova T.**, **Higashi T.**, **Balakova R.** A "weird" mitochondrial fatty acid oxidation as a metabolic "secret" of cancer. ***Oxid. Med. Cell. Longev.***, 2022; **2022**: 2339584. doi:10.1155/2022/2339584. PMCID: PMC8847026, PMID: 35178152.

71 **Varelas X.**, **Bouchie M. P.**, **Kukuruzinska M. A.** Protein N-glycosylation in oral cancer: dysregulated cellular networks among DPAGT1, E-cadherin adhesion and canonical Wnt signaling. ***Glycobiology***, 2014; **24**(7): 579–591. doi:10.1093/glycob/cwu031. PMID: 24742667. PMCID: PMC4038253.

72 **Bansil R.**, **Yannas I. V.**, **Stanlay H. E.** Raman spectroscopy: a structural probe of glycosaminoglycans. ***Biochim. Biophys. Acta***, 1978; **541**: 536–542.

73 **Tsukamoto S.**, **Takahama T.**, **Mavrogenis A. F.**, **Tanaka Y.**, **Tanaka Y.**, **Errani C.** Clinical outcomes of medical treatments for progressive desmoid tumors following active surveillance: a systematic review. ***Musculoskelet. Surg.***, 2022. doi:10.1007/s12306-022-00738-x.

74 **Battaglia A. G.**, **Ali-Zade C.**, **Monti L.**, **Al Khawashki H.**, **Winkler H.**, **Del Sel H.**, **Mavrogenis A. F.**, **Benzakour T.**, **Drago L.**, **Romanò C. L.** World association against infection in orthopedics and trauma (W.A.I.O.T.) study group on bone and joint infection definitions. Metal hypersensitivity or missed periprosthetic joint infection? A critical review. ***Orthopedics***, 2022; 1–6. doi:10.3928/01477447-20211227-04. PMID: 34978510.

75 **Tsantes A. G.**, **Papadopoulos D. V.**, **Trikoupis I. G.**, **Tsante K. A.**, **Mavrogenis A. F.**, **Koulouvaris P.**, **Vaiopoulos A. G.**, **Piovani D.**, **Nikolopoulos G. K.**, **Kokoris S. I.**, **Bonovas S.**, **Papagelopoulos P. J.**, **Tsantes A. E.** The prognostic performance of rotational thromboelastometry for excessive bleeding and increased transfusion requirements in hip fracture surgeries. ***Thromb. Haemost.***, 2021. doi:10.1055/s-0041-1736617.

76 **Tsukamoto S.**, **Errani C.**, **Kido A.**, **Mavrogenis A. F.** What's new in the management of metastatic bone disease. ***Eur. J. Orthop. Surg. Traumatol.***, 2021; **31**(8): 1547–1555.

77 **Tsukamoto S.**, **Kido A.**, **Tanaka Y.**, **Facchini G.**, **Peta G.**, **Rossi G.**, **Mavrogenis A. F.** Current overview of treatment for metastatic bone disease. ***Curr. Oncol.***, 2021; **28**(5): 3347–3372. https://doi.org/10.3390/curroncol28050290.

78 **Syngouna S. A.**, **Mitsikostas P.**, **Sioutis S.**, **Bekos A.**, **Fandridis E.**, **Mavrogenis A. F.**, **Tsiodras S.**, **Pneumaticos S. G.** Diagnostic value of IL-1β, IL-17A, and IL-17F serum levels in patients with upper extremity infections. ***J. Long Term Eff. Med. Implants***, 2021; **31**(4): 39–44.

79 **Errani C.**, **Mavrogenis A. F.**, **Tsukamoto S.** What's new in musculoskeletal oncology. ***BMC Musculoskelet. Disord.***, 2021; **22**(1): 704.

80 **Errani C.**, **Bazzocchi A.**, **Spinnato P.**, **Facchini G.**, **Campanacci L.**, **Rossi G.**, **Mavrogenis A. F.** What's new in management of bone metastases? ***Eur. J. Orthop. Surg. Traumatol.***, 2019; **29**(7): 1367–1375.

81 **Kokkalis Z. T.**, **Iliopoulos I. D.**, **Antoniou G.**, **Antoniadou T.**, **Mavrogenis A. F.**, **Panagiotopoulos E.** Posterior shoulder fracture-dislocation: an update with treatment algorithm. ***Eur. J. Orthop. Surg. Traumatol.***, 2017; **27**(3): 285–294. doi:10.1007/s00590-016-1840-5. PMID: 27562590.

82 **Mavrogenis A. F.**, **Angelini A.**, **Errani C.**, **Rimondi E.** How should musculoskeletal biopsies be performed?. ***Orthopedics***, 2014; **37**(9): 585–588. doi:10.3928/01477447-20140825-03. PMID: 25198351.

83 **Mavrogenis A. F.**, **Angelini A.**, **Vottis C.**, **Palmerini E.**, **Rimondi E.**, **Rossi G.**, **Papagelopoulos P. J.**, **Ruggieri P.** State-of-the-art approach for bone sarcomas. ***Eur. J. Orthop. Surg. Traumatol.***, 2015; **25**(1): 5–15. doi:10.1007/s00590-014-1468-2.

84 **Ruggieri P.**, **Mavrogenis A. F.**, **Mercuri M.** Quality of life following limb-salvage surgery for bone sarcomas. ***Expert Rev. Pharmacoecon. Outcomes Res.***, 2011; **11**(1): 59–73. ISSN: 1744-8379.

85 **Ruggieri P.**, **Mavrogenis A. F.**, **Casadei R.**, **Errani C.**, **Angelini A.**, **Calabrò T.**, **Pala E.**, **Mercuri M.** Protocol of surgical treatment of long bone pathological fractures. ***Injury***, 2010; **41**(11): 1161–1167. doi:10.1016/j.injury.2010.09.018. PMID: 20947077.

86 **Kumar S.**, **Srinivasan A.**, **Nikolajeff F.** Role of infrared spectroscopy and imaging in cancer diagnosis. ***Curr. Med. Chem.***, 2018; **25**(9): 1055–1072. doi:10.2174/0929867324666170523121314.

87 **Brandenburg K.**, **Kusumoto S.**, **Seydel U.** Conformational studies of synthetic lipid A analogues and partial structures by infrared spectroscopy. ***Biochim. Biophys. Acta (BBA)***, 1997; **1329**: 183–201.

88 **Anastassopoulou J.**, **Kyriakidou M.**, **Kyriazis S.**, **Kormas T. H.**, **Mavrogenis A. F.**, **Dritsa V.**, **Kolovou P.**, **Theophanides T.** An FT-IR spectroscopic study of metastatic cancerous bone. In: Theophanides T. (ed.), Infrared Spectroscopy-Anharmonicity of Biomolecules, Crosslinking of Biopolymers, Food Quality and Medical Applications. London: InTech Open, 2015; pp. 89–100, Chapt. 5.